Eur. Phys. J. B **7**, 551–562 (1999)

THE EUROPEAN PHYSICAL JOURNAL B

EDP Sciences

High magnetic field properties and ESR of the $Li_{1-z}Ni_{1+z}O_2$ compounds

A.-L. Barra[1], G. Chouteau[1,a], A. Stepanov[2], A. Rougier[3], and C. Delmas[3]

[1] Grenoble High Magnetic Field Laboratory[b], MPI - FKF and CNRS, B.P. 166, 38042 Grenoble Cedex 09, France
[2] Laboratoire MATOP, Faculté Saint-Jérôme, C-151,Université Aix-Marseille III, 13397 Marseille Cedex 20, France
[3] Institut de Chimie de la Matière Condensée de Bordeaux-ICMCB-CNRS, et École Nationale Supérieure de Chimie et Physique de Bordeaux, avenue Dr. A. Schweitzer, 33608 Pessac Cedex, France

Received: 24 July 1998 / Revised and Accepted: 23 September 1998

Abstract. $Li_{1-z}Ni_{1+z}O_2$ compounds have a layered structure made of alternating Ni-O and Li-O slabs. An amount z of extra divalent Ni ions is always present in the Li-O layers. We show, using high field magnetisation, static and dynamic susceptibility and high frequency ESR, that the magnetic properties are driven by the z parameter. The compounds can be described as ferromagnetic Ni-O layers, bridged by clusters possessing a net ferromagnetic moment.

PACS. 75.25.+z Spin arrangements in magnetically ordered materials (including neutron and spin-polarized electron studies, synchrotron-source X-ray scattering, etc.) – 75.30.Et Exchange and superexchange interactions – 76.50.+g Ferromagnetic, antiferromagnetic, and ferrimagnetic resonances; spin-wave resonance

1 Introduction

Lithium nickel oxide, $LiNiO_2$, has been reported for the first time by Dyer *et al.* [1]. This material can be considered as the end member ($z = 0.5$) of the $Li_zNi_{1-z}O_2$ solid solution which was previously studied in order to understand the effect of the presence of divalent nickel ions in nickel oxide [2]. The layered structure of $LiNiO_2$ and the low spin state of trivalent nickel ions in this material have raised a considerable interest of physicists for this material which can be considered as a $S = 1/2$ triangular lattice model. However, as it will be discussed in the following many results and interpretations of the literature are contradictory. This results from the departure to the ideal stoichiometry always present in this material. Small amounts of Ni atoms substitute to Li ones in the Li layers. This substitution is accompanied by a valence change of the Ni ions from +3 to +2. The amount of Ni^{2+} strongly depends on the preparation conditions. The knowledge of the $Ni^{2+}Ni^{3+}$ ratio is the key to understand the magnetic properties. In Table 1 we give an overview of the main results published in the literature along with the various interpretations of the magnetic properties. It is worth noting the anomalously large ordering temperature published by some authors [9], was simply due to an underestimation of the real amount of Ni^{2+} in the compound studied.

Recently, a strong renewal of interest on $LiNiO_2$ has occurred since this material is a very promising positive electrode material for lithium-ion batteries [22–24]. Its electrochemical behaviour allows its use (or some of its derivatives) in batteries for electrical vehicle. The battery capacity is very sensitive to the departure from the ideal stoichiometry, therefore, numerous studies have been devoted to the syntheses optimisation, to the structural characterisation through the Rietveld refinement method [25,26].

In this paper we present a systematic study of the $Li_{1+z}Ni_{1-z}O_2$ series in which z was intentionally varied from 0.02, which is one of the purest compound ever published, up to 0.25.

2 Materials characterisation

2.1 Synthesis

The $Li_{1-z}Ni_{1+z}O_2$ phases considered in this paper were obtained by direct syntheses under an oxygen flow from a mixture of Li_2O and NiO. Two thermal treatments (600 °C for 10 h and 700 °C for 15 h) are necessary to obtain pure well-crystallised phases. To evidence the effect of the high temperature treatment on lithium nickelate a series of thermal treatments (600 °C for 6 days, 700 °C for 15 h, 800 °C for 15 h, 850 °C for 15 h and 950 °C for 15 h) was

[a] e-mail: chouteau@labs.polycnrs-gre.fr
[b] Laboratoire conventionné avec l'Institut National Polytechnique, Grenoble, et l'Université Joseph-Fourier, Grenoble 1.

Table 1. Description of the main results and interpretation of the literature.

Authors	Ref.	Experiment	Interpretation of the magnetic properties
Goodenough *et al.* 1958	[3]	$M(T)/H$	$Li_x^+Ni_{1-2x}^{2+}Ni_x^{3+}O$ $x < 0.3$ antiferromagnet $x > 0.3$ ferrimagnet Ni^{3+} in the low spin state All Ni-O-Ni interactions antiferromagnetic
Hirakawa 1985, 1990	[4]	$M(H)$, ESR, neutrons	Possible quantum spin liquid
Itoh *et al.* 1986	[5]	NMR on ^7Li	$LiNiO_2$ nominal two anomalies at $T_{N1} = 210$ K and $T_{N2} = 20$ K ferro or ferrimagnetism below T_{N2}
Hirota *et al.* 1990, Hirota *et al.* 1991 Hirota *et al.* 1992	[6] [7] [8]	$M(H)$, $\chi_{ac}(T)$, $C(T)$, neutrons	$LiNi_{1-z}Co_zO_2$, Ni^{3+} in the low spin state $LiNiO_2$ 2D triangular frustrated magnet antiferromagnetic **intralayer** exchange interaction between next nearest and nearest neighbours weak ferromagnetic **interlayer** interaction
Stoyanova *et al.* 1993	[9]	X-band ESR	$Li_{0.96}Ni_{1.04}O_2$ and $LiNi_zCo_{1-z}O_2$ 2D Heisenberg ferromagnet crossover at 30 K from Heisenberg to ZY Ni^{3+} in the low spin state
Reimers *et al.* 1993	[10]	$M(H)$, time effects	$Li_zNi_{2-z}O_2$ Ni^{2+} in the Li layers antiferromagnetic 2D frustrated triangular system with ferromagnetic interlayer interactions, spin glass
Yamaura *et al.* 1996	[11]	$M(H)$, $\chi_{dc}(T)$	$Li_{1-z}Ni_{1+z}O_2$ spin glass $z < 0.01$ ferromagnet $z > 0.01$ ferromagnetic Ni-Ni **intralayer** interaction ferromagnetic Ni-Ni **interlayer** interaction orbital frustration Ni^{3+} in the low spin state $LiNiO_2$ is a triangular ferromagnet
Bajpai *et al.* 1997	[12]	$\chi_{ac}(T)$ linear and non-linear, $\chi_{dc}(T)$	$Li_{1-z}Ni_{1+z}O_2$ $z = 0.3$ and 0.35, spin glass
Rougier *et al.* 1996 Barra *et al.* 1997	[13] [14]	$M(H)$, $\chi_{dc}(T)$, $\chi_{ac}(T)$, X-band and high field ESR	$Li_{1-z}Ni_{1+z}O_2$, Ni^{3+} in the low spin state frustrated 2D triangular antiferromagnet for $z \to 0$ assembly of ferro or ferrimagnetic **clusters** for $z > 0$
Azzoni *et al.* 1996	[15]	$M(H)$, $\chi_{dc}(T)$, ESR	Two phases present: $Li_zNi_{1-z}O$ diluted antiferromagnet, $Li_{2z}Ni_{2-2z}O_2$ ferrimagnet Ni^{3+} in the low spin state
Ohta *et al.* 1997	[16]	High field ESR	$z = 0.004$ and .054, ferromagnetic internal field
Yoshizawa *et al.* 1990	[19]	SANS	existence of short range order

done starting from a $Li_2O + 2NiO$ mixture. In these conditions a lithium deficient disordered phase was obtained.

All these phases were characterised by Rietveld refinement (Fullprof program), [27]. Magnetic properties were investigated using high field (up to 12 T), and low field magnetisation measurements, ac susceptibility, zero field and field cooled dc susceptibility and X-band, Q-band and high frequency ESR. We used powdered compacted samples contained in ultra pure, (99.999%), cylindrical copper sample holders. The size of the samples was typically 5 mm in diameter and 2 to 3 mm in length.

2.2 Structural characterisation

All these materials crystallise in the rhombohedral system ($R{-}3m$ space group). The detailed structural study and preparation of all samples considered in this paper have been previously reported [25,27], therefore, only the results interesting for the further magnetic characterisation are considered here.

The structure is schematically represented in Figure 1. The lithium/nickel ordering in the (111) planes of the fcc oxygen packing leads to the ideal structure of $LiNiO_2$

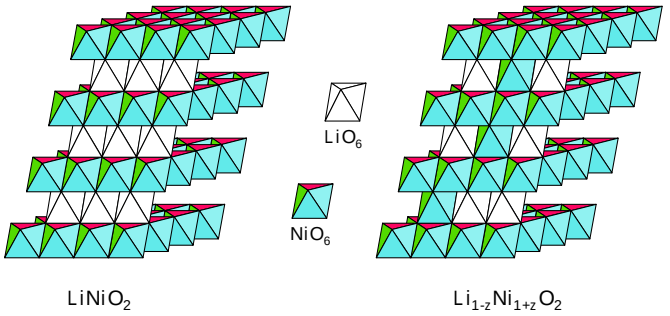

Fig. 1. Left: $LiNiO_2$ structure. Right: $Li_{1-z}Ni_{1+z}$ structure showing the substitution of Ni in the Li layers.

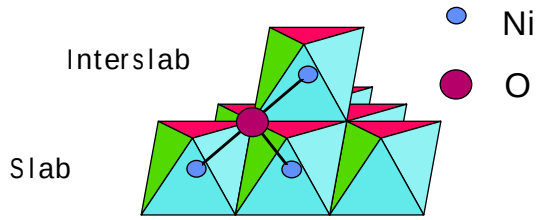

Fig. 2. Structure of the Ni-O slab showing the 180°and the 90°O-Ni-O bonds.

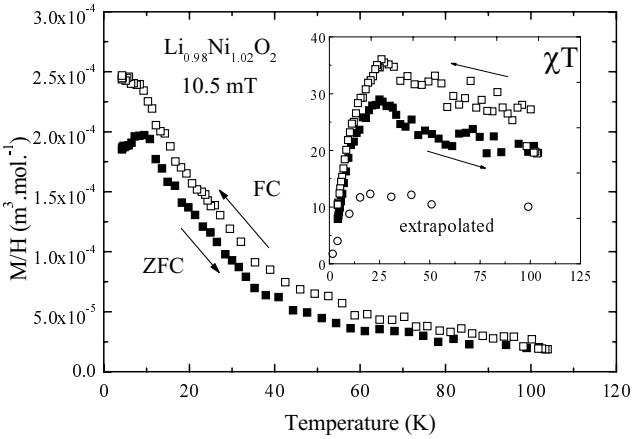

Fig. 3. ZFC and FC static susceptibility of the "matrix" $Li_{0.98}Ni_{1.02}O_2$. Insert χT *vs.* T diagram. Open dots are deduced from Arrott's plot analysis (see text).

which can be also described from a packing of NiO_2 slabs built up of edge-sharing NiO_6 octahedra. In fact, extra nickel ions are always present in the lithium site as also shown in Figure 1 leading to the $Li_{1-z}Ni_{1+z}O_2$ composition. As we have previously discussed, the X-ray diffraction is very sensitive to the presence of nickel ion within the lithium plane, but cannot detect the presence of a small amount of lithium in the nickel plane resulting of an hypothetical disorder. Neutrons diffraction experiments recently performed on $Li_{1-z}Ni_{1+z}O_2$ ($z \leq 0.25$) phases obtained at 700 °C shows that there is no Li/Ni mixing or in other words that there is no lithium ions in the NiO_2 slabs [28].

The composition of the materials obtained at 700 °C are $Li_{0.98}Ni_{1.02}O_2$, $Li_{0.94}Ni_{1.06}O_2$, $Li_{0.88}Ni_{1.12}O_2$ and $Li_{0.76}Ni_{1.24}O_2$. The comparison of the octahedra size in the slab and in the interslab space suggests that the z nickel ions of the interslab space are divalent. In order to achieve the material electroneutrality there are also z divalent ions in the NiO_2 slabs. Moreover, the local charge compensation (2nd Pauling rule) requires that the divalent nickel ions of the slab remain in the vicinity of the interslab ones. Therefore, for these four materials the crystallographic formula can be written $\left(Li_{1-z}Ni_z^{II}\right)_{interslab}\left(Ni_z^{II}Ni_{1-z}^{III}\right)_{slab}O_2$ with $z = 0.02$, 0.06, 0.12 and 0.24. One cannot exclude a recharging of the $O\,2p$ states instead of the $3d$ Ni states as commonly admitted [29]. The fifth compound characterised in this work was obtained at very high temperature and exhibits a Li/Ni mixing in addition to the stoichiometry departure. The compilation of the results concerning the chemical analysis, the X-ray Rietveld refinement and the specific mass determination shows that its overall chemical formula $Li_{0.75}Ni_{1.25}O_2$ leads to the following crystallographic one $(Li_{0.64}Ni_{0.36})_{interslab}(Li_{0.11}Ni_{0.89})_{slab}O_2$. The presence of lithium in the slab and of a large amount of nickel in the interslab space leads to a rhombohedral cell which is very close to the cubic one as evidenced by the c/a ratio of the hexagonal axes (equal to 4.906). This value is very close to the ideal one (4.90) in absence of a rhombohedral distortion. For the four previously described phases which are clearly rhombohedral, c/a ranges between 4.933 and 4.924 when z increases from 0.02 to 0.24. For the $(Li_{0.64}Ni_{0.36})_{interslab}(Li_{0.11}Ni_{0.89})_{slab}O_2$ phase the distribution of divalent and trivalent nickel ions in the two types of sites is an open question. Nevertheless, contrary to other phases, both cations must exist in both sites.

As far as magnetic interactions are concerned it is important to consider the orbital overlap in the structure. Within the NiO_2 slab there are only 90° Ni-O-Ni interactions (Fig. 2), which, according to Goodenough rules should be ferromagnetic. Only these interactions are observed in $NaNiO_2$ or in ideal $LiNiO_2$. On the contrary in the case of the $Li_{1-z}Ni_{1+z}O_2$ lithium deficient phase the presence of nickel ions in the interslab space introduce 180° Ni-O-Ni superexchange interactions with the Ni ions in the Ni-O slabs which strongly modify the magnetic properties, since they are antiferromagnetic.

3 Magnetism

3.1 Matrix properties

3.1.1 Magnetisation and susceptibility

Let us first focus on the less concentrated compound $Li_{1.02}Ni_{0.98}O_2$. In Figure 3 we have plotted the static susceptibility measured under a 10.5 mT field, in the temperature range 4–100 K. Open squares are for the field cooled, (FC), experiment and black ones for the zero field cooled one, (ZFC). The difference between the two curves is small, within the experimental accuracy. This shows that the remnant magnetisation is very weak proving

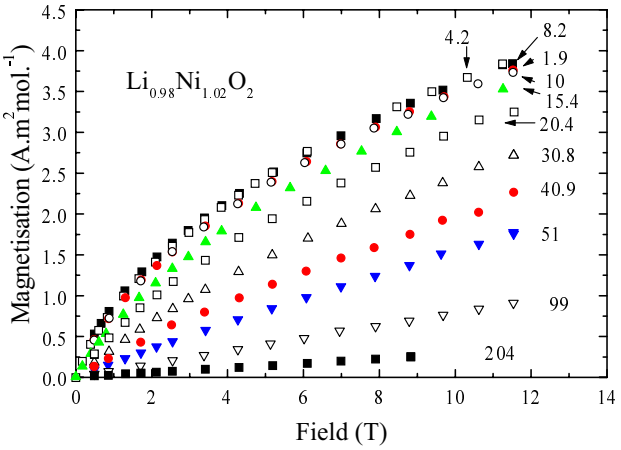

Fig. 4. Magnetisation isotherms for the $Li_{0.98}Ni_{1.02}O_2$ compound, up to 12 T. Temperatures in Kelvin are indicated in the figure.

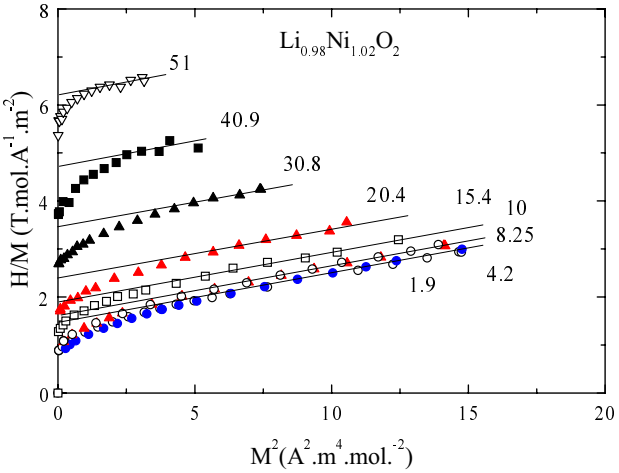

Fig. 5. Arrott's plots of the $Li_{0.98}Ni_{1.02}O_2$ compound showing the trend to homogeneity in high fields: high field parts of the isotherms are parallel straight lines.

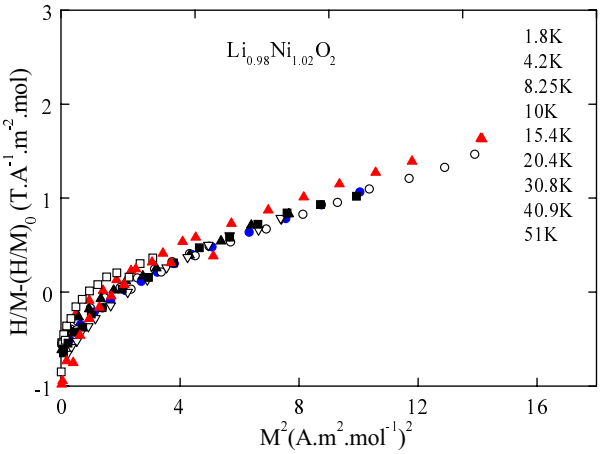

Fig. 6. Reduced Arrott's plot for the $Li_{0.98}Ni_{1.02}O_2$ compound.

the absence of long range ferromagnetic order. The hysteresis loop recorded between −200 mT and +200 mT, at 4.2 K, shows a very narrow cycle, confirming this fact, (Fig. 13).

The tendency towards a Curie law at high temperature is evidenced in the $\chi T(T)$ diagram, (insert in Fig. 3). However no Curie constant can be determined unambiguously even at 100 K. To get the real Curie-Weiss law it is necessary to make measurements well above 100 K, [17]. This is also true for more concentrated compounds and explains why wrong values of the Curie constants have been often published.

The magnetisation isotherms are drawn in Figure 4. No saturation is present even in fields as high as 12 T at 1.9 K. It is well known that the Arrott's plots [18] are a good way of finding the ordering temperature, if any, and also to determine whether the magnetic system is homogeneous or not, that is whether the magnetisation density is uniform in the whole volume or not. In Arrott's model for $M \ll M_S$ where M_S is the saturation magnetisation, one has,

$$\frac{H}{M} = \frac{1}{\chi} + aM^2 \qquad (1)$$

with $1/\chi = (T - T_C)/C$, where T_C is the ordering temperature and C the Curie constant. The coefficient a in equation (1) is temperature independent for uniform systems, but is strongly temperature dependent in disordered systems or spins glasses [21]. Therefore, in the plot H/M *vs.* M^2 the magnetisation isotherms should be straight lines. Their intercept with vertical axis is positive for $T > T_C$ and negative for $T < T_C$. The critical isotherm at $T = T_C$ has a zero intercept. For uniform magnetic systems these lines are parallel.

Figure 5 shows that this is verified for high field magnetisation, indicating that $Li_{0.98}Ni_{1.02}O_2$ becomes uniform in high fields. Low field curvatures indicate the existence of small inhomogeneities, which are the signature of magnetic clusters or short-range order. Anisotropy and demagnetising field effects can also exist but are of little importance. More sophisticated plots near T_C can be used in order to determine the critical exponent of the magnetisation [19], however in the present case Figure 5 clearly shows that the ordering temperature is much lower than 1.9 K, in the Arrott's sense.

In order to get more information about the homogeneous state we have plotted the intercept of the high field straight lines of Arrott's plots $(H/M)_0$, (see Fig. 5), as a function of temperature, (Fig. 3, open squares, curve labelled "extrapolated"). A Curie-Weiss law is obtained ($\theta \approx 18$ K) with a flattening off below ≈ 20 K. The extrapolated Curie constant $C_{ext} \approx 0.56$ emu.mol^{-1}, ($\mu_{eff} = 2.1\ \mu_B$), corresponds roughly to the effective moment of Ni^{3+} in the low spin state. It is smaller than the Curie constant measured in a 10.5 mT field, $C = 1.31$ emu.mol^{-1}, ($\mu_{eff} = 3.24\ \mu_B$). This is what is expected if the system is made of small clusters, pairs or triplets, which are not saturated in low fields but saturated in high fields or

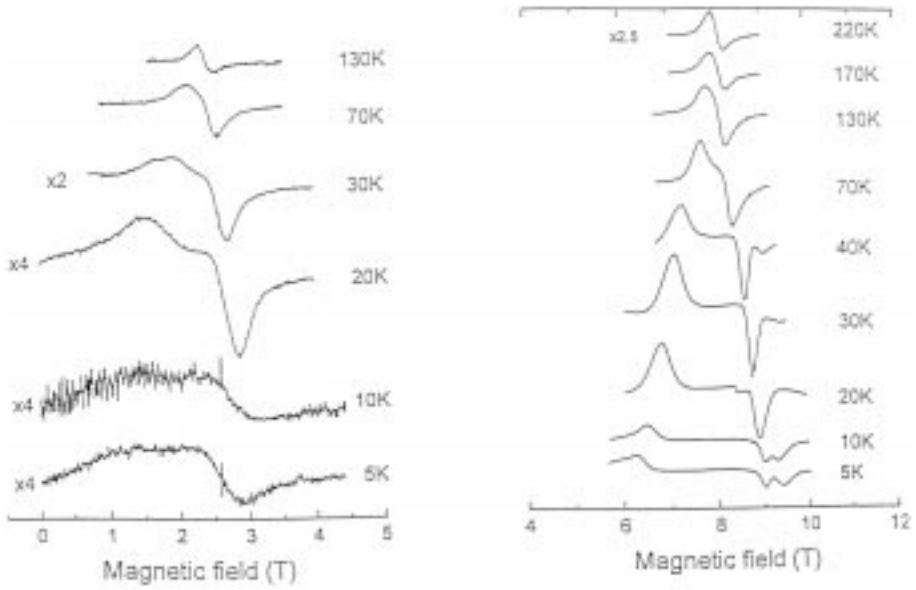

Fig. 7. ESR spectra for the $Li_{0.98}Ni_{1.02}O_2$ compound. Left: 73 GHz, right: 246 GHz.

if it exhibits short range order, in agreement with SANS experiments [20].

It is worth noticing that the plot $H/M - (H/M)_0$ *vs.* M^2 gives a unique curve in the whole range of temperatures and fields showing that the temperature dependence of the magnetisation only comes from the Curie term $(H/M)_0$ while the a parameter in equation (1) is field dependent and temperature independent (Fig. 6), as expected for homogeneous systems.

3.1.2 ESR

Ni^{2+} has an integer spin $S = 1$. Because of large spin-orbit coupling the ESR line width is so large that no resonance can be observed in the range 15–300 K. In addition, for low z the number of Ni^{2+} ions is too small to be observable even at low temperatures. Therefore the ESR signal is mainly due to Ni^{3+} ions which possess a spin $S = 1/2$ in the low spin state. Conventional X-band spectroscopy at 9.5 GHz shows a single line at $g = 2.02$ at 300 K and $g = 2.06$ at 10 K. Its width is around 0.2 T. ESR spectra recorded at 73 GHz and 245 GHz at various temperatures, Figure 7, show quite different behaviours. At high temperatures a single symmetric line is observed at $g = 2.15$. Below 130 K two lines appear corresponding to two anisotropic g factors. Analysing these resonances by use of the usual formula $g_{eff} = 1/3g_{\|} + 2/3g_{\perp}$ one finds $g_{\perp} < g_{\|}$. The difference $g_{\|} - g_{\perp}$ increases as $T \to 0$. At $T = 20$ K we find $g_{\|} = 3.15$ and $g_{\perp} = 1.8$. Below 20 K the lines intensity rapidly decreases on cooling and the lines seem to become noisy. The behaviour of the ESR lines is very peculiar. Below 20 K it corresponds probably to the existence of a weak antiferromagnetic phase, in agreement with magnetic measurements. At higher temperatures local dynamic Jahn-Teller, could explain it. From the above results we conclude that ideal $LiNiO_2$ would be a two dimensional system with no long-range magnetic order. Static and dynamic Jahn-Teller effects play also an important role. The question of which Hamiltonian is appropriate to describe this system is still open. Very careful magnetisation and susceptibility measurements are needed to clarify this point.

3.2 Cluster regime

The magnetic behaviour of compounds exhibiting a significant departure from stoichiometry, ($z > 0.02$), is quite different. As z increases, the magnetisation isotherms exhibit stronger curvatures. Above $z = 0.06$ a clear saturation of M appears at moderate fields, (2 to 3 T), although a high field susceptibility remains, (Figs. 8 to 11). For $z = 0.12$, 0.24 and 0.25, ($z + y = 0.36$), one can unambiguously determine the saturation magnetisation M_S by extrapolating to $H = 0$ the high field linear part of the magnetisation curves. For $z = 0.06$ and $z = 0.02$ this procedure is more questionable due to the continuous curvature of the $M(H)$ curves. In Figure 12 are plotted the $M_S(z)$ values. In a very simplified model, M_S can be written,

$$M_S = z\mu(Ni^{2+}) + (1 - z)\mu(Ni^{3+}). \qquad (2)$$

Equation (2) assumes that Ni^{2+} and Ni^{3+} moments align independently under a magnetic field. However Ni^{2+} ions in the lithium layers are linked to the Ni^{3+} slabs through a very strong 180° Ni-O-Ni antiferromagnetic superexchange bound which is about the same as in NiO. They cannot saturate in a 12 T field and their contribution to M_S is thus negligible. Only the second term of equation (2) should be taken into account. This gives the straight line in Figure 12. Taking into account also the Ni^{2+} contribution would give the dashed line in Figure 12. We made the additional assumption that Ni^{3+} is in the low spin state [30].

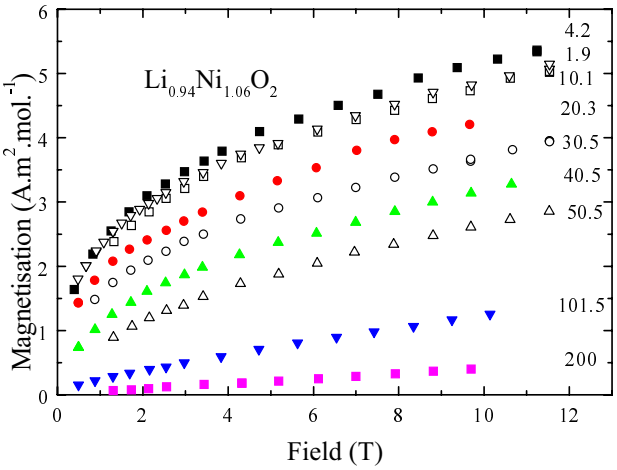

Fig. 8. Magnetisation isotherms for the $Li_{0.94}Ni_{1.06}O_2$ compound, up to 12 T. Temperatures in Kelvin are indicated in the figure.

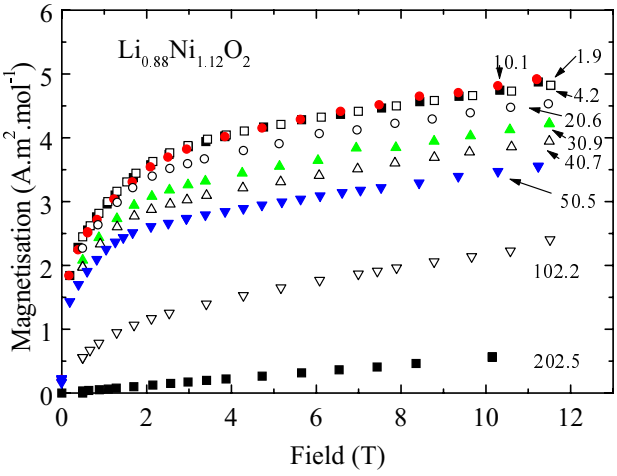

Fig. 9. Magnetisation isotherms for the $Li_{0.88}Ni_{1.12}O_2$ compound, up to 12 T.

Clearly the measured M'_S do not follow equation (2). For $z < 0.12$ they are much smaller than the calculated values. This is in agreement with the idea of magnetic clusters [31]. For $z > 0.24$ another departure from the straight line occurs, but it is due to a change in the chemical structure. Indeed, for the $z = 0.25$ nominal composition a significant amount of lithium ions substitute Ni ions in the Ni-O slabs, so that the relative concentration of Ni ions in the lithium site is increased. Although the average chemical formula is always $Li_{1-z}Ni_{1+z}O_2$ the true crystallographic one is $(Li_{0.64}Ni^{2+}_{0.36})(Li_{0.11}Ni^{2+}_{0.14}Ni^{3+}_{0.75})O_2$. In this material there are 0.50 Ni^{2+} ions and 0.75 Ni^{3-} ions. The rhombohedral distortion is very weak in comparison to other phases and one can thus assume that divalent and trivalent nickel ions are distributed over both types of sites.

Ferromagnetic correlations are obvious in the magnetisation curves. The shape of the hysteresis loops at 4.2 K also confirms their presence (Fig. 13). They show striking features. For $z = 0.06$ and $z = 0.12$ no saturation

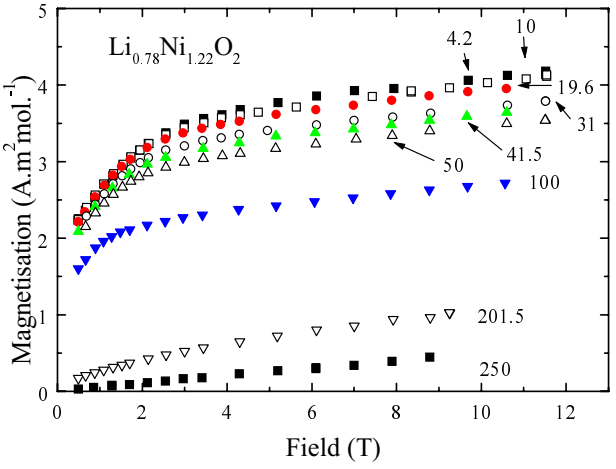

Fig. 10. Magnetisation isotherms for the $Li_{0.76}Ni_{1.24}O_2$ compound, up to 12 T.

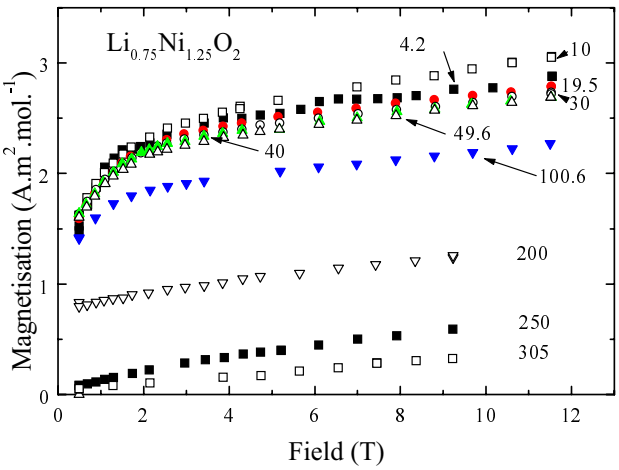

Fig. 11. Magnetisation isotherms for the $Li_{0.75}Ni_{1.25}O_2$ compound, up to 12 T.

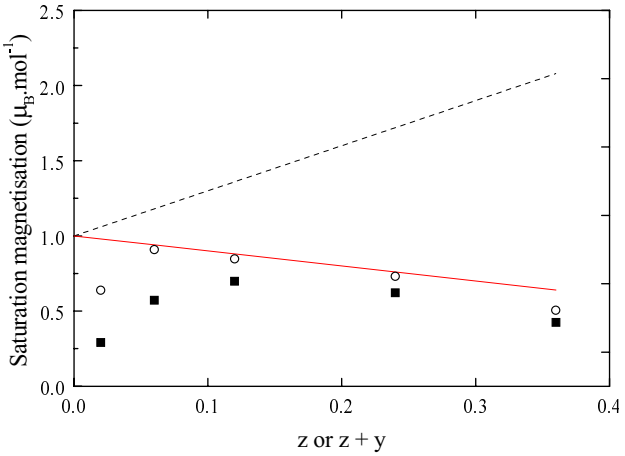

Fig. 12. Saturation magnetisation of the $Li_{1-z}Ni_{1+z}O_2$ family deduced from the high field part of the magnetisation curves. The straight lines are fits to equation (2), (see text).

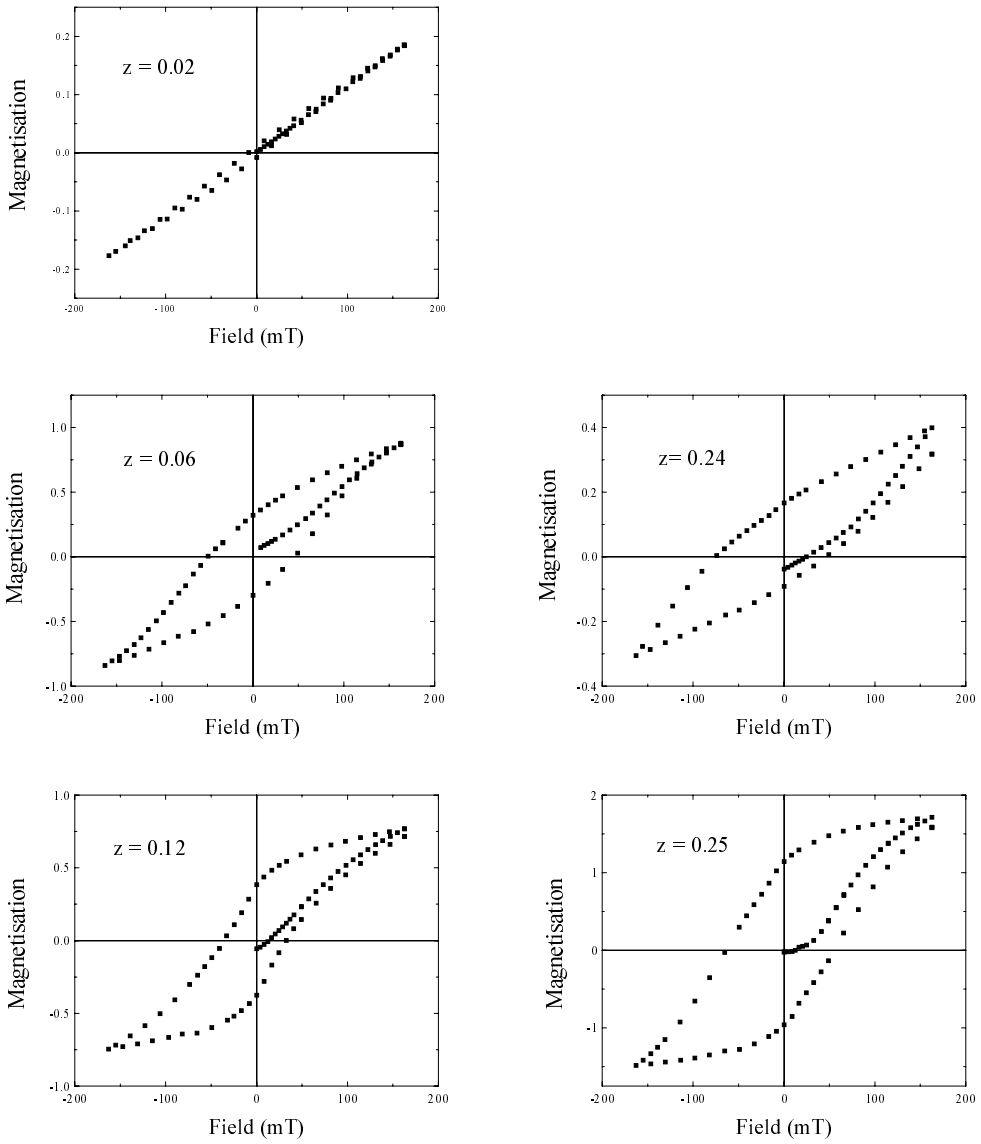

Fig. 13. Hysteresis loops showing the different regimes as a function of z: $z = 0.02$ "matrix", $z = 0.06$ and 0.12 non interacting clusters, $z = 0.24$ interacting clusters, (non symmetric cycle), $z = 0.25$ real 0.36, long range order.

is observed and the coercive field increases with z. This is in agreement with a model of independent ferromagnetic clusters. In such a case the hysteresis loop is symmetric and is the sum of all the individual loops. For $z = 0.24$ we observe a very different shape and in particular the loop is very asymmetric. This is the proof of the existence of important interactions between clusters. They act as if an additional field to the applied field existed. Finally for $z = 0.25$ the loop is again symmetric with a clear tendency to saturation as is observed in long range ferromagnets. However, the absence of a horizontal plateau in high field, even for the highest values of z and the continuous curvatures of M *vs.* H prove the absence of a well defined long range order. This is evidenced in the Arrott's plots, (Figs. 14 to 17), which exhibit stronger and stronger curvatures as z increases, and can no longer be described by equation (1).

One can attempt to define the ordering temperature T_C^A from the high field linear part of Arrott's plots, (see Figs. 14 to 17), as explained above. Results are gathered in Table 2, and plotted in Figure 18, in a logarithmic scale. The straight dashed line intercepts the horizontal axis at $z = z_C \approx 0.06$. Below this critical concentration $T_C^A \approx 0$. The existence of a threshold for z is an additional indication of the presence of clusters since z_C can be interpreted as a percolation threshold which means that beyond z_C one can find at least one cluster with an infinite size.

Another way of describing the onset of ferrimagnetic ordering is to study the susceptibility. Different behaviours appear as z increases. For $z = 0.02$ and 0.06, no well-defined anomaly exists. The $\chi(T)$ curves are characterised by a very small difference between χ_{FC} and χ_{ZFC} as seen before. In addition they exhibit a very long high temperature "tail", indicative of the onset of a progressive

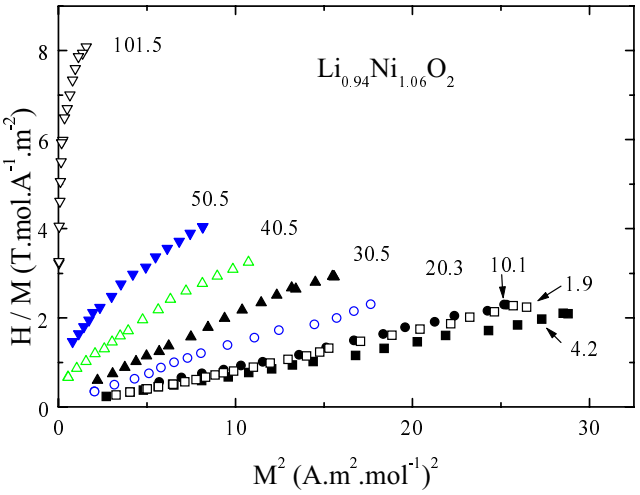

Fig. 14. Arrott plot for the $Li_{0.94}Ni_{1.06}O_2$ compound.

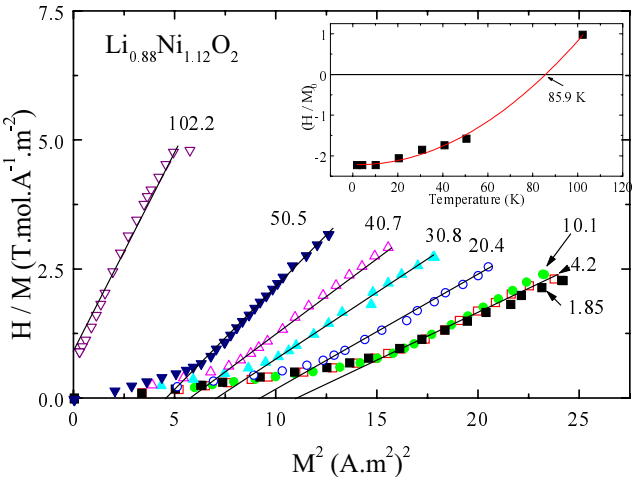

Fig. 15. Arrott plot for the $Li_{0.88}Ni_{1.12}O_2$ compound. Straight lines are linear high field extrapolations from which the ratio $(H/M)_0$ is deduced. The insert shows how the ordering temperature is obtained with the plot of $(H/M)_0$ *vs.* T. The continuous line is a polynomial interpolation of the points. Note that negative values of $(H/M)_0$ have no physical meaning. They are used just for the polynomial fit.

Table 2. Ordering temperatures deduced from Arrott's plots (T_C^A(K)), and from the susceptibility, (T_C^χ(K)).

z or $(z+y)$	T_C^A(K)	T_C^χ(K)
0.02	< 1.9	40
0.06	5	57.5
0.12	85.9	102
0.22 (0.24)	161	188
0.25 (0.36)	210	239

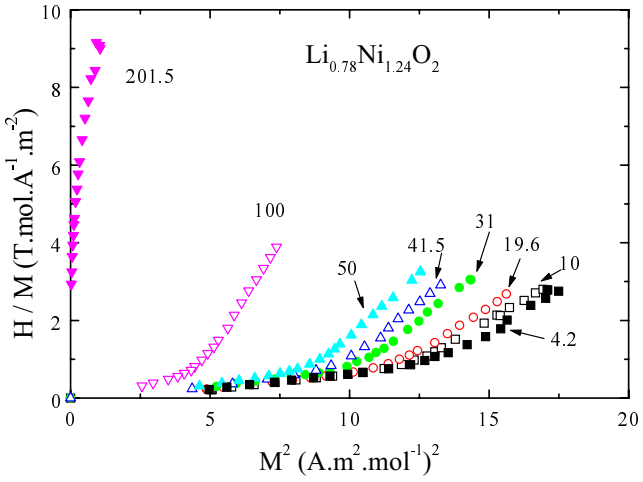

Fig. 16. Arrott plot for the $Li_{0.76}Ni_{1.24}O_2$ compound.

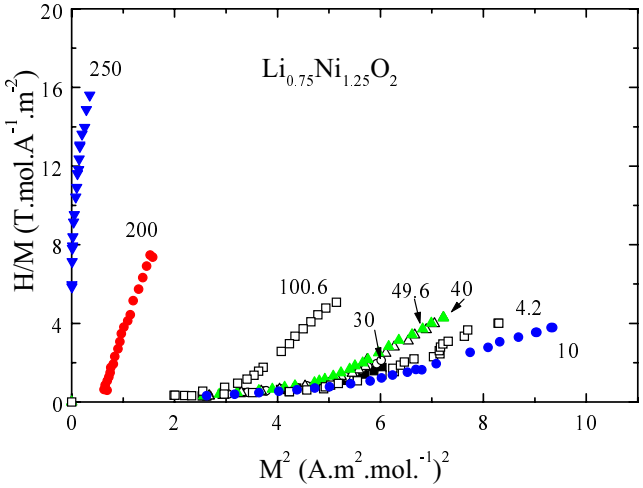

Fig. 17. Arrott plot for the $Li_{0.75}Ni_{1.25}O_2$ compound.

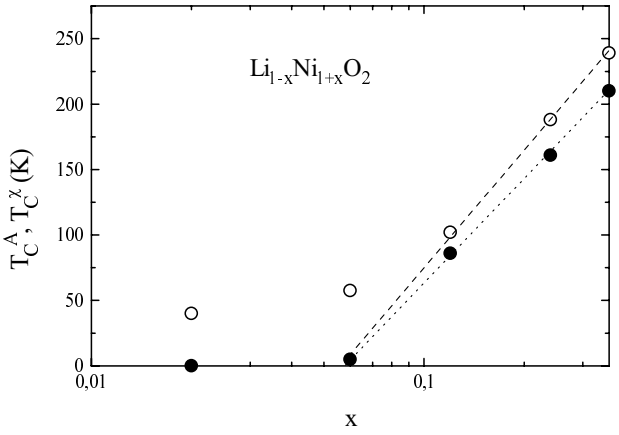

Fig. 18. ordering temperatures obtained using different criteria, showing the existence of a critical concentration at $z_C \approx 0.06$.

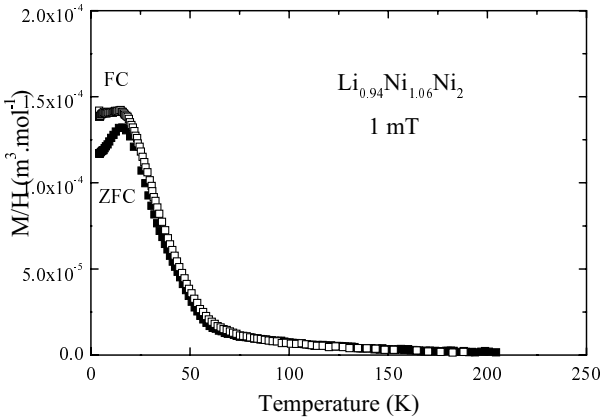

Fig. 19. Static susceptibility, (1 mT), for the $Li_{0.94}Ni_{1.06}O_2$ compound. Black squares: FC, open squares: ZFC. The maximum in the ZFC curve is due to the blocking temperature of the clusters rather than to an antiferromagnetic order.

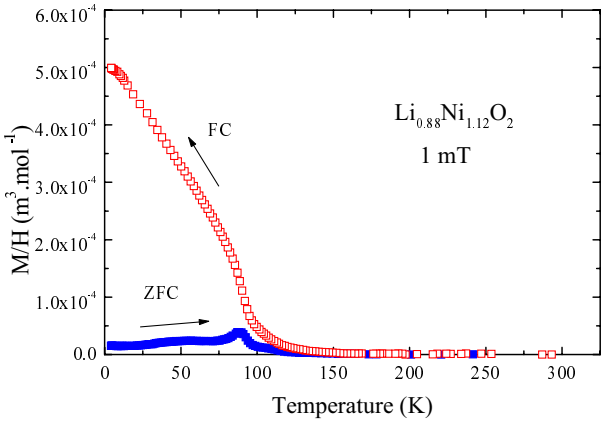

Fig. 20. Static susceptibility, (1 mT), for the $Li_{0.88}Ni_{1.12}O_2$ compound. Black squares: ZFC, open squares: FC. Note the huge effect of a small applied field on the FC curve.

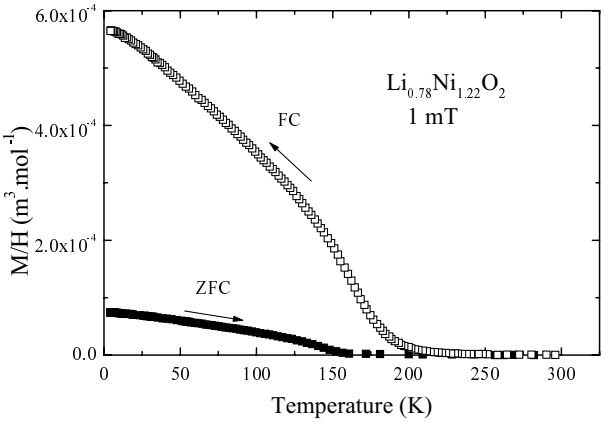

Fig. 21. Static susceptibility, (1 mT), for the $Li_{0.78}Ni_{1.22}O_2$ compound. Black squares: ZFC, open squares: FC.

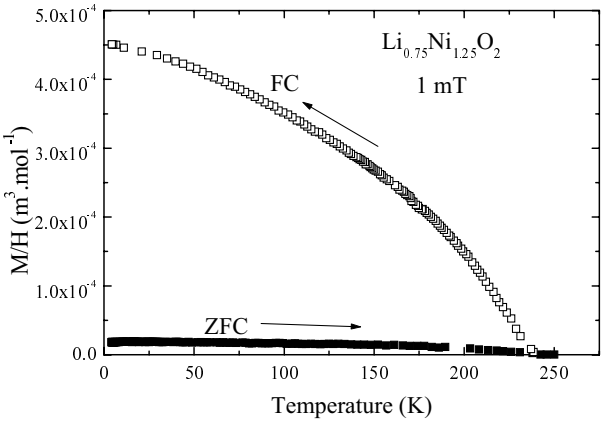

Fig. 22. Static susceptibility, (1 mT), for the $Li_{0.75}Ni_{1.25}O_2$ compound. Black squares: ZFC, open squares: FC. The shape of the ZFC curve is typical for a long range ordering.

ordering, analogous to a spin glass freezing. The maximum in $\chi(T)$ curves at lower temperature, (8 K for $z = 0.02$ and 15 K for $z = 0.06$), is typical of the behaviour of ferromagnetic clusters around their blocking temperature (Fig. 19).

For $z = 0.12$ and $z = 0.22$ one observes a more abrupt change of χ below a given temperature, although a high temperature tail still exists (Figs. 20, 21). The main difference with the two preceding compounds is the huge difference between χ_{FC} and χ_{ZFC}. A very small applied field of 1 mT is enough to induce a very large remnant magnetisation M_R. For instance for $z = 0.12$, M_R at 4.2 K equals $\approx 10\%\, M_S$. This is the sign that ferromagnetism is induced in these compounds.

Finally the most concentrated compound, with $z = 0.25$ which contains 0.36 nickel ion in the Li sites, exhibits a true phase transition at $T_C = 239$ K, with almost no "tail" and an even larger induced ferromagnetism than the former compounds, (Fig. 22). We can consider this compound as a real long range ferrimagnet with only small short range order. In this particular case every nickel ion in the interslab space is antiferromagnetically coupled to the Ni ions of the slabs. Within this model the saturation magnetisation, assuming an equal number of Ni^{2+} ions in the slabs and in the interslab space, should be

$$\lfloor 0.64\mu(Ni^{3+}) + 0.25\mu(Ni^{2+})\rfloor_{slab} - \lfloor 0.11\mu(Ni^{3+}) + 0.25\mu(Ni^{2+})\rfloor_{interslab} = 0.53\mu_B$$

in good agreement with experiment.

We define the "ordering temperature", T_C^χ from χ measured in a 1 mT field, as the intercept of the inflection point tangential with the temperature axis, (second column of Table 2, and open circles in Fig. 18). Although T_C^χ is not well defined for $z = 0.02$, we observe the same behaviour than for T_C^A, namely the existence of the same threshold at $z \approx 0.06$ and a steep increase above this concentration. One always observes $T_C^\chi > T_C^A$. This is a field effect. Indeed, the biggest clusters order, (freeze), at higher temperatures and contribute essentially to the low field susceptibility while small clusters are only visible in high fields.

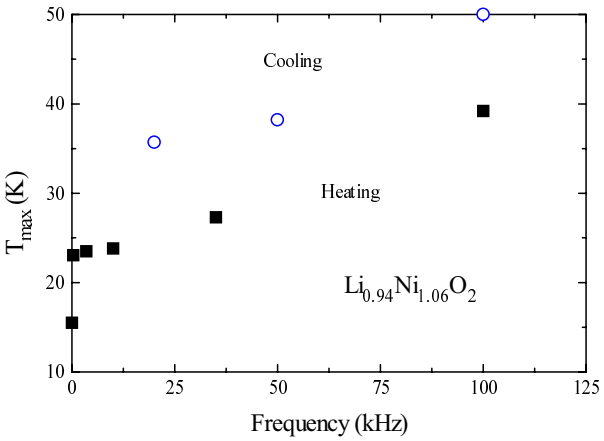

Fig. 23. Effect of the frequency on the temperature of the maximum of χ_{ac}.

At this point we can picture the $Li_{1-z}Ni_{1+z}O_2$ family as follows. Very low concentration compounds can be described as an assembly of almost non interacting ferromagnetic clusters imbedded in the $LiNiO_2$ matrix. In agreement with Goodenough's rules and recent calculations using a mean field model [31], or Monte-Carlo simulations [32], the Ni-O-Ni interactions in the Ni^{3+} slabs are weakly ferromagnetic. The size of the clusters is distributed over a wide range as proved by the long tail of the $\chi(T)$ curves. As z increases, the number of these clusters increases, but they remain independent, because $T_C \propto z$. At $z = z_C$ the interactions between clusters become important, and probably a percolation threshold occurs. This means that large ordered domains exist in the compound above z_C explaining the rapid increase of T_C with z. Above the nominal composition $z = 0.25$, (real $z = 0.36$), the compounds are long range ordered ferrimagnets.

In disordered systems, like spin glasses, the magnetic state is not at thermodynamic equilibrium and more or less complex relaxation effects are often observed [10]. An assembly of superparamagnetic clusters should also exhibit relaxation effects. We have measured the ac susceptibility of the $Li_{0.94}Ni_{1.06}O_2$ compound as a function of the frequency in the range 337 Hz–100 kHz. The $\chi_{ac}(T)$ curves have a maximum at $T_{max}(\omega)$. Figure 23 shows that $T_{max}(\omega)$ is an increasing function of ω as expected for a cluster assembly or a spin glass [21]. This is in agreement with reference [10] where authors have observed a double exponential decay of the magnetisation of their compounds after a field cooling. In fact, in disordered systems there is always a distribution of the relaxation times. In our experiments the ω dependence of T_{max} depends whether the temperature is swept up or down (Fig. 23), probably because short time (in the ms or μs range) and long time (a few hours), relaxation effects are simultaneously present.

In order to confirm the above general analysis we have investigated the ESR response of the $Li_{0.94}Ni_{1.06}O_2$ compound in which the amount of clusters is large enough to be easily detected. In Figure 24 are plotted the spectra recorded between 5 K and 300 K at 78 and 246 GHz. At room temperature and at 78 GHz, a slightly asymmetric line is observed at $g = 2.17$. This line splits into two lines at 235 K. One line remains temperature independent on cooling while the other one moves towards the highest fields. Around 120 K two new lines appear which move in opposite directions as the temperature decreases. It is worth noticing that the intensity is every times redistributed over the lines. This is quite typical of ferro(ferri)magnetic resonance. Indeed, for a ferrimagnetic cluster two modes appear at the Curie temperature. One shifts towards the lower fields. It corresponds to the case of the field applied parallel to the easy axis. The second ones shifts towards the higher fields. It corresponds to the field applied perpendicular to the hard axis. In the case of powdered samples both signals are seen simultaneously. At low temperatures the modes which appeared at 120 K exhibit a very large gap of 70 GHz with $g_{\|} = 2.4$ and $g_{\perp} = 2.17$. We observe that the gap value does not depend on the z parameter, which is an indication of its non magnetic origin. All these features are also observed at 246 GHz, the only difference being a larger splitting of the modes. The same qualitative behaviour was also seen for the $Li_{0.88}Ni_{1.12}O_2$ compound, which contains much more numerous clusters, at 56 and 246 GHz, (Fig. 25).

In order to understand the striking behaviour of the ESR response and the existence of a very strong enhanced ferromagnetism above $z = 0.06$, it is necessary to keep in mind that the NiO_6 octahedra are systems with potentially strong Jahn-Teller effect, especially in the case of d^7Ni^{3+} ions in the low spin state. As is well-known, two distortions of the octahedra can occur along the tetragonal axis. One is an elongation and the other one is compression. Each one corresponds to a particular ground state; ($|x^2-y^2\rangle$ and $|3z^2-r^2\rangle$ respectively). At low temperature and in high fields $g_{\|}$ is larger than $g_{\perp}$ which is the case when $|x^2-y^2\rangle$ orbital is the ground state. At high temperature only one component is observed, which is the average $g = 1/3(g_{\|} + 2g_{\perp})$. This is in favour of a *dynamic Jahn-Teller effect*. However when the temperature is decreased, the dynamic Jahn-Teller effect generally transforms into the static one. Applying a magnetic field tends to stabilise the $|x^2-y^2\rangle$ orbital which favours ferromagnetic coupling between Ni^{3+} ions.

4 Conclusion

We have shown, using a careful Rietveld analysis that the structure of the $LiNiO_2$ is strongly affected by the preparation conditions. We have prepared the purest $LiNiO_2$ compound with only 2% of extra nickel ions in the lithium layers.

Our main conclusions are the following. Stoichiometric $LiNiO_2$ if it existed would be a superposition of weak ferromagnetic Ni^{3+} layers. The most concentrated sample with $z = 0.25$, ($z + y = 0.36$), is a 3D ferrimagnet exhibiting a true long-range order. Each Ni^{2+} ion in the lithium layer couples antiferromagnetically to six nearest

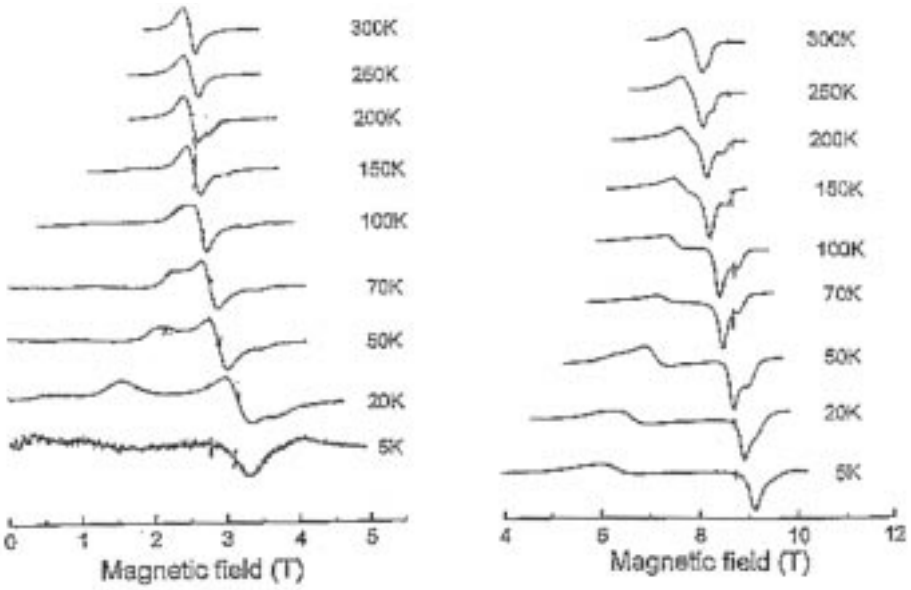

Fig. 24. ESR spectra for the $Li_{0.94}Ni_{1.06}O_2$ compound showing the appearance of two lines ferro(ferri)magnetic resonance lines below 235 K and 120 K. Left: $f = 78$ GHz, right: $f = 246$ GHz.

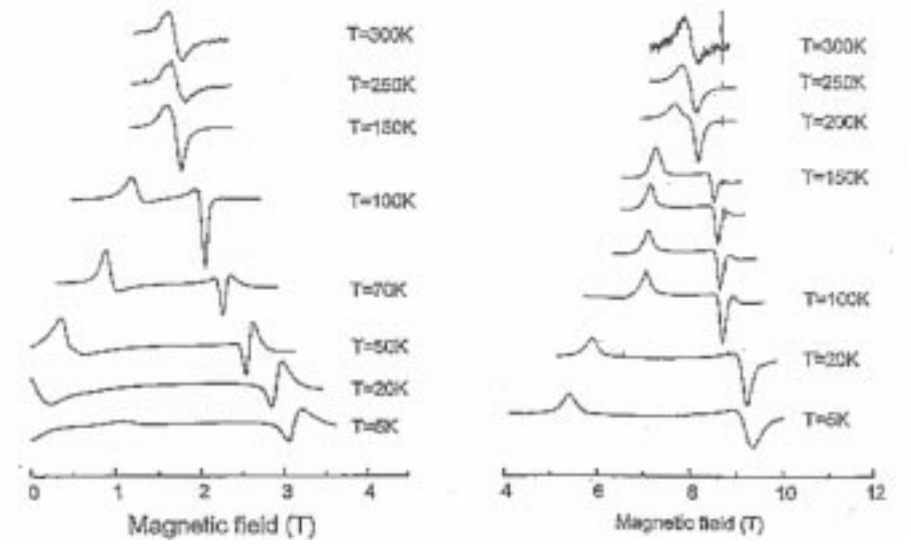

Fig. 25. ESR spectra for the $Li_{0.88}Ni_{1.12}O_2$ compound. Left: $f = 52.6$ GHz, right: $f = 246$ GHz.

Ni^{3+} ions in the two adjacent layers, forming a ferrimagnetic cluster. For intermediate values of z, magnetic properties are dominated by the existence of these clusters, which can be considered independent for low z values.

The magnetic properties evolve from a quasi-2D paramagnet with an ordering temperature well below 1.9 K, for $z = 0.02$, towards a true long-range ferrimagnet for $z = 0.25$, $(z + y = 36)$.

ESR experiments show that Jahn-Teller effect plays a crucial role in the stabilisation of the ferrimagnetic ground state. The long range ordered state observed above $z = 0.25$, $(z + y = 36)$ is ferrimagnetic rather than ferromagnetic because in case of a pure ferromagnet the change in the $\chi(T)$ curve below T_C would be much steeper. This confirms the antiferromagnetic nature of the Ni^{3+}-O-Ni^{2+} interactions.

References

1. L.D. Dyer, B.S. Borie Jr, G.P. Smith, J. Am. Chem. Soc. **20**, 1499 (1954).
2. E.J.W. Verwey, P.W. Haayman, F.C. Romeyn, G.W. Oosteriaut, Chem Weekblad **44**, 705 (1948); Philips Research Report **5**, 173 (1950).
3. J.B. Goodenough, D.J. Wicham, W.J. Croft, J. Chem. Solids **5**, 107 (1958).
4. K. Hirakawa, H. Kadowaki, K. Ubukoshi, J. Phys. Soc. Jpn **54**, 3526 (1985); K. Hirakawa, R. Osborn, A.T. Taylor, K. Takeda, J. Phys. Soc. Jpn **59**, 3081 (1990).
5. M. Itoh, I. Yamada, K. Ubukushi, K. Hirakawa, H. Yasuoka, J. Phys. Soc. Jpn **55**, 2125 (1986).
6. K. Hirota, Y. Nakazawa, H. Yoshizawa, J. Magn. Magn. Mater. **90-91**, 279 (1990).
7. K. Hirota, Y. Nakazawa, M. Ishikawa, J. Phys-Cond. **3**, 4721 (1991).
8. K. Hirota, H. Yoshizawa, M. Ishikawa, J. Phys-Cond. **4**, 6291 (1992).
9. R. Stoyanova, E. Zhecheva, C. Friebel, J. Phys. Chem. Solids **54**, 9 (1993).
10. J.N. Reimers, J.R. Dahn, J.E. Greedan, C.V. Stager, G. Liu, I. Davidson, U. von Sacken J. Solid State Chem. **102**, 542 (1993).
11. K. Yamaura, M. Takano, A. Hirano, R. Kanno, J. Solid State Chem. **127**, 109 (1996).
12. A. Bajpai, A. Banerjee, Phys. Rev. B **55**, 12439 (1997).
13. A. Rougier, C. Delmas, G. Chouteau, J. Phys. Chem. Solids **57**, 1101 (1996).
14. A.L. Barra, G. Chouteau, A. Stepanov, C. Delmas, to appear in J. Magn. Magn. Mater.
15. C.B. Azzoni, A. Paleari, M. Massarotti Bini, D. Capsoni, Phys. Rev. B **53**, 703 (1996).
16. H. Ohta, Y. Yamamoto, Y. Ikeuchi, M. Motokawa, A. Hirano, R. Kanno, Physica B **237-238**, 64 (1997).
17. A. Rougier, Thesis, Bordeaux University (1995).
18. A. Arrott, Phys. Rev. **108**, 1394 (1957).
19. A. Arrott, J.E. Noakes, Phys. Rev. Lett. **19**, 786, (1967).
20. H. Yoshizawa, H. Mori, K. Hirota, M. Ishikawa, J. Phys. Soc. Jpn **59**, 2631 (1990).
21. See for instance the review paper of K. Binder, A.P. Young, Rev. Mod. Phys. 58, 801 (1980).
22. G. Demazeau, N. Chevreau, L. Founès, J.L. Soubeyroux, Y. Takeda, M. Thomas, M. Pouchard, Rev. Chim. Min. **20**, 155 (1983).
23. J.R. Dahn, U. von Sacken, C.A. Michal, Solid State Ionics **44**, 87 (1990).
24. M. Broussely, F. Perton, P. Biensan, J.M. Bodet, J. Labat, A. Lecerf, C. Delmas A. Rougier, J.P. Peres, J. Power Sources **54**, 109 (1995).
25. A. Rougier, P. Gravereau, C. Delmas, J. Electrochem. Soc. **143**, 1168 (1996).
26. R. Kanno, H. Kubo, Y. Kawamoto, T. Kamiyama, F. Izumi, Y. Takeda, M. Takano, J. Solid State Chem. **110**, 216 (1994).
27. J. Rodrigues-Carvajal, *Collected Abstracts of Powder diffraction Meeting*, Toulouse, France (1990), p. 127.
28. J.P. Pérès, E. Suard, T. Chaterji, C. Louchet, C. Delmas, Proceedings of GFECI 98, Font-Romeu, France (1998).
29. P. Kuiper, G. Kruizinga, J. Ghijsen, G.A. Sawatzky, Phys. Rev. Lett. **62**, 221 (1989).
30. Note that according to reference [29] there is no difference from the magnetic point of view between Ni^{3+} in the low spin state and O2p hole states.
31. M.D. Nuñez-Regueiro, E. Chappel, G. Chouteau, C. Delmas, *Proceedings of SCES 98*, Paris 15-18 July 1998, to appear in Physica B.
32. J.M. Debièvre, F. Celestini, MATOP/CNRS, Université Marseille-III, private communication.